The effect of the solar rotational irradiance variation on the middle and upper atmosphere calculated by a three-dimensional chemistry-climate model

A. N. Gruzdev, H. Schmidt, G. P. Brasseur

Atmos. Chem. Phys. Discuss., 8, 1113–1158, 2008
www.atmos-chem-phys-discuss.net/8/1113/2008/

Atmospheric Chemistry and Physics Discussions

The effect of the solar rotational irradiance variation on the middle and upper atmosphere calculated by a three-dimensional chemistry-climate model

A. N. Gruzdev[1], **H. Schmidt**[2], **and G. P. Brasseur**[3]

[1]A. M. Obukhov Institute of Atmospheric Physics, Moscow, Russia
[2]Max-Planck-Institut für Meteorologie, Hamburg, Germany
[3]National Center for Atmospheric Research, Boulder, CO, USA

Received: 28 November 2007 – Accepted: 7 December 2007 – Published: 23 January 2008

Correspondence to: H. Schmidt (hauke.schmidt@zmaw.de)

Abstract

This paper analyzes the effects of the solar rotational (27-day) irradiance variations on the chemical composition and temperature of the stratosphere, mesosphere and lower thermosphere as simulated by the three-dimensional chemistry-climate model HAMMONIA. Different methods are used to analyze the model results, including high resolution spectral and cross-spectral techniques. Shortcomings of the frequently applied correlation (regression) method are revealed. To force the simulations, an idealized irradiance variation with a constant period of 27 days (apparent solar rotation period) and with constant amplitude is used. While the calculated thermal and chemical responses are very distinct and permanent in the upper atmosphere, the responses in the stratosphere and mesosphere vary considerably in time despite the constant forcing. The responses produced by the model exhibit a non-linear behavior. In general, the response sensitivities decrease with increasing amplitude of the forcing. In the extratropics the responses are, in general, seasonally dependent with frequently stronger sensitivities in winter than in summer. Amplitude and phase lag of the ozone response in the tropical stratosphere and lower mesosphere are in satisfactory agreement with available observations, while discrepancies between calculated and observed ozone responses become larger above ~75 km. The agreement between the calculated and observed temperature response is generally worse than in the case of ozone.

1 Introduction

The variation of solar radiation reaching the Earth atmosphere with a period of approximately 27 days is caused by the longitudinally inhomogeneous distribution of magnetic field structures on the surface of the rotating Sun. The magnitude of this variation is spectrally dependent and varies with time. It is typically one third of the variation observed over an 11-year solar cycle.

The tropospheric response to the 27-day variation of the Sun is very small and often

ACPD

8, 1113–1158, 2008

undetectable. However, a 27-day solar induced signal is clearly identifiable in the middle and upper atmosphere. The unambiguous identification of the response to solar variations on the 11-year and longer time scales requires the analysis of very long time-series. These are not easily available. Knowledge on amplitude and phase characteristics of the response of the atmospheric thermal structure and chemical composition to the 27-day solar forcing is easier to derive and is useful for better understanding atmospheric photochemical processes. Because the periods of the 27-solar variation and of its superharmonics are close to the typical periods of wave-like disturbances occurring in the middle atmosphere, the possible interaction of the solar and planetary wave signals is an interesting issue.

Effects of the 27-day solar cycle on temperature and chemical composition of the middle atmosphere were studied through analyses of space observations that mainly concentrated on ozone and temperature responses in low latitudes (e.g. Hood, 1984, 1986, 1987; Gille et al., 1984; Chandra, 1985; Keating et al., 1985, 1987; Eckman, 1986b; Hood and Cantrell, 1988; Hood et al., 1991; Chandra et al., 1994; Fleming et al., 1995; Zhou et al., 1997, 2000; Hood and Zhou, 1998; Ruzmaikin et al., 2007). Keckhut and Chanin (1992) analyzed Rayleigh lidar temperature data. To retrieve the 27-day signal in these atmospheric quantities, different methods were used: spectral analysis and filter techniques for the identification of 27-day signals, correlation and cross-spectral analysis for estimating the phase (time lag) of a signal relative to the solar radiation variations, averaging, spectral analysis, and linear regression analysis for estimating the amplitude and sensitivity of a response to changes in solar radiation.

Most observational studies show that the maximum sensitivity (and amplitude) of the tropical stratospheric ozone response occurs at about 40 km altitude. The maximum ozone response to a 1% change in solar radiation at the wavelength of 205 nm (i.e. the sensitivity) varies from 0.2 to 0.6% (Hood, 1984, 1986; Hood and Cantrell, 1988; Hood et al., 1991; Hood and Zhou, 1998, 1999; Zhou et al., 2000). The phase lag of the tropical stratospheric ozone response depends on altitude. Several studies suggest that ozone lags solar forcing by a few days at an altitude of 30 km, but leads the forcing

by a few days at an altitude of 50 km (Keating et al., 1985, 1987; Eckman, 1986b; Hood, 1986, 1987; Hood and Cantrell, 1988; Fleming et al., 1995; Zhou et al., 1997; Hood and Zhou, 1998). Fewer studies are available for the mesosphere. However, most of them indicate that the sensitivity of the ozone response increases with height above 55–65 km altitude (Keating et al., 1985; Eckman et al., 1986b; Keating et al., 1987; Hood et al., 1991). At 65–75 km, the ozone response is approximately in opposite phase with the variations in solar irradiance (Keating et al., 1987; Hood et al., 1991; Chandra et al., 1994; Fleming et al., 1995).

Observations suggest that the maximum response of the tropical temperature to the 27-day solar variation occurs between 50 and 60 km (Hood, 1986, 1987; Hood and Cantrell, 1988; Keckhut and Chanin, 1992; Chen et al., 1997; Hood and Zhou, 1998), or even at about 70 km (Keating et al., 1987; Keckhut and Chanin, 1992). The maximum sensitivity of the upper stratospheric temperature response is of the order of 0.16 K per 1% change in solar radiation at 205 nm (Hood, 1986, 1987; Hood and Cantrell, 1988; Hood and Zhou, 1998). There are however significant differences between the phase lags of temperature responses derived from different data sets. The lag at the maximum response altitude varies from 4–7 days for Nimbus SAMS data (Hood, 1986, 1987; Keating et al., 1987; Hood and Cantrell, 1988) to near zero in the case of lidar and UARS MLS data (Keckhut and Chanin, 1992; Hood and Zhu, 1998).

Numerical simulations of the tropical ozone and temperature responses to the 27-day solar forcing have been performed with 1-dimensional (Eckman, 1986a; Brasseur et al., 1987; Summers et al., 1990; Chen et al., 1997), 2-dimensional (Brasseur, 1993; Fleming et al., 1995; Chen et al., 1997; Zhu et al., 2003) and 3-dimensional (Williams et al., 2001; Rozanov et al., 2006) photochemical-dynamical models. Generally, the characteristics of the model results for stratospheric and lower mesospheric responses are consistent with the relatively broad ranges derived from experimental data. However, one should note significant differences in the results obtained with different 2-dimensional models (Fleming et al., 1995; Chen et al., 1997; Zhu et al., 2003). Furthermore, using a 3-dimensional chemistry-climate model, Williams et al. (2001) found

ACPD
8, 1113–1158, 2008

a negative lag for the temperature response in the upper stratosphere, which contradicts most two-dimensional model results and observational studies. In the case of the middle mesosphere, significant differences in amplitude and phase exist between simulated (Summers et al., 1990; Chen et al., 1997) and observed temperature responses.

In this paper, we present results of several simulations performed with the three-dimensional chemistry-climate model HAMMONIA (Hamburg model of the neutral and ionized atmosphere). The response of temperature, ozone, and related chemical species to the 27-day cycle forcing is analyzed from the surface to the lower thermosphere. One of the objectives of this paper is to study the time and latitude dependence of the atmospheric response and thereby to provide a more complete picture than most of earlier studies which concentrated primarily on the equatorial region. Another aim of the present study is to assess the respective merits of different analysis methods that are used to identify 27-day solar signals. Applying a variety of methods to analyze numerical experiments performed with and without 27-day solar forcing allows us to identify possible misinterpretations that may occur using for example methods based on the widely-used correlation technique. It will be shown that the model produces variations with periods in the vicinity of 27 days also in simulations that do not include a 27-day forcing. Further, we will present a case of a possible interference of the 27-day signal with atmospheric wave disturbances of a period close to 16 days, and we will describe non-linearities associated with the atmospheric response.

Section 2 provides a brief description of the numerical model and of the different simulations. The methods for the analysis of the model results are described in Sect. 3. The solar forcing data are presented in Sect. 4. In Sect. 5, we discuss the results of the numerical experiments and compare them to observations. Conclusions can be found in Sect. 6.

2 Description of the model

HAMMONIA is a global 3-dimensional chemistry-climate model extending from the surface to the thermosphere with the upper boundary at about 250 km. It is an extension towards higher altitudes of the ECHAM5 (Roeckner et al., 2003, 2006) and MAECHAM5 (Giorgetta et al., 2006; Manzini et al., 2006) general circulation models. Several new parameterizations had to be implemented in HAMMONIA in order to account for important processes that occur in the mesosphere and thermosphere (e.g. solar heating at wavelengths down to 5 nm, non-LTE effects in the infrared cooling, heating in the near-infrared CO_2 bands, molecular heat conduction and diffusion of tracers, and the ion drag). As the model includes a full formulation of tropospheric dynamics and physics, it is producing internal variability in a wide range of frequencies. It has been shown that the model variability compares well with observed atmospheric variability in the cases of the northern winter stratosphere (Manzini et al., 2006), and of the global mesosphere and lower thermosphere (Offermann et al., 2007). The model dynamics and physics are interactively coupled with the MOZART3 chemistry scheme (Kinnison et al., 2007) that includes 48 compounds and 153 gas phase reactions in this version. HAMMONIA has already been applied for studying the atmospheric response to the 11-year solar cycle (Schmidt et al., 2006; Schmidt and Brasseur, 2006). A detailed model description is given by Schmidt et al. (2006).

As in the latter study, the model is run with a spectral truncation of T31 (corresponding approximately to a horizontal resolution of 3.75×3.75 degrees) with 67 layers in the vertical. We have performed three 6-year simulations of which we interpret only the last 5 years. The cases reported here are the following:

- S0: without 27-day variation in solar forcing,
- S27: with a 27-day forcing of realistic amplitude,
- S27*3: with a 27day forcing with tripled amplitude (only in the spectral range 120–740 nm).

ACPD
8, 1113–1158, 2008

The latter case is used to improve the signal-to-noise ratio for an easier identification of the response and to study its non-linearity.

The 27-day variation in spectral extraterrestrial solar irradiance $S_\lambda(t)$ from the extreme UV to the infrared is used as an input parameter at the upper model boundary. This variation is prescribed as a sinusoidal 27-day oscillation around the mean (depending on latitude and time of year) spectral solar fluxes $S_{0,\lambda}$:

$$S_\lambda(t) = S_{0,\lambda} + A_\lambda \sin(t/27).$$

Here, t is the time in days (set to zero for 1 January, 00:00 UT, of the first interpreted year of the simulations). The wavelength-dependent amplitude, A_λ, of this variation is calculated as described in Sect. 4, and kept constant during the entire model integration.

For convenience, model results are presented as a function of geometric altitude. However, this quantity represents a pseudo-pressure coordinate because it is calculated from model pressure coordinates using latitude dependent 5-year annual mean vertical temperature distributions.

3 Methods of analysis

The model results are analyzed by different methods. The purpose of the analysis is not only to detect a 27-day signal in the atmosphere and calculate its amplitude and phase characteristics, but also to prove that the detected atmospheric response is related to the solar forcing. We begin with relatively simple methods such as the correlation and filter techniques used in many previous studies. Subsequently we apply different high resolution spectral methods.

To smooth the time series and remove the annual and semi-annual cycles and long-term changes, high and low-frequency Kaiser-Bessel filters and their combination (as a band pass filter) are used (Harris, 1978).

ACPD
8, 1113–1158, 2008

Linear correlation and regression coefficients are calculated for different time shifts between the filtered time series and the solar forcing. The correlation coefficients are analyzed in Sect. 5.1, while ozone and temperature sensitivities to the 27-day forcing, which are estimated as maximum regression coefficients, are discussed in Sect. 5.7.

To estimate amplitudes and periods of variations within a broad range of time scales, and to analyze their time evolution, a wavelet transform technique is used (Sect. 5.2). In order to exclude loss of data at the edges (beginning and end) of the time series, the series are continued beyond the edges with an autoregression approach (Gruzdev and Bezverkhny, 2000, 2005).

To study the spectral composition of the time series, the high resolution spectral analysis method suggested by Bezverkhny (1986; see also Gruzdev and Bezverkhny, 2000, 2005) is used. The method provides an estimate of the spectral density by applying an autoregression filtering and a Fourier decomposition into spheroid wave eigenfunctions.

Together with the spectral analysis, we use a spectral-time analysis which is an application of a spectral method for shorter time periods within a running window. In particular, this approach allows to assess the time evolution of power spectra and the seasonal dependence and interannual variability of the spectral composition of a signal. Compared to a wavelet analysis, spectral-time analysis provides a better spectral resolution, while the wavelet analysis reveals individual variations.

Running and seasonally averaged ozone and temperature spectra are analyzed in Sect. 5.3. Spectral-time analysis of solar flux data is presented in Sect. 4.

If spectral analysis reveals a dominating oscillation in a time series, Fourier harmonic analysis can be used to calculate amplitudes and phases of this oscillation and its superhamonics as done for the solar flux data in Sect. 4.

The results of the spectral analysis are further used to estimate the amplitudes of the atmospheric responses to the solar forcing. Since an integration of a spectrum over frequency gives a variance of a time series (Jenkins and Watts, 1968), integration over a frequency band in the neighborhood of a sharp spectral peak gives a variance of

variations with periods corresponding to this spectral maximum. The square root of this variance is related to the mean amplitude of the respective variations. Theoretically, the variance of a sinusoidal signal is equal to the squared amplitude multiplied by a factor of two. However in our case of in general non-sinusoidal signals we use a heuristically obtained factor. The variance corresponding to a spectral peak is calculated by integrating a power spectrum over a frequency range limited by the frequencies corresponding to half of the maximum spectral density. The factor needed to derive the amplitude from the variance is calculated applying this method to the spectrum of a sinusoidal signal. We derived this factor for recalculation of square root variance to amplitude of a signal (Sect. 5.5).

Further, we use a high-resolution cross-spectral analysis based on the maximum entropy method (Jones, 1978) to check whether or not atmospheric 27-day variations are related to the 27-day solar forcing. In particular, coherence and phase spectra are considered. The spectral coherence can be interpreted as a correlation coefficient between two time series defined at each frequency (Jenkins and Watts, 1968). The phase spectrum gives a phase difference (time lag) between two time series for each frequency. The model as well as real atmosphere produces variability within a broad frequency range, so that not all variations with periods close to 27 days are necessarily related to solar forcing. We consider such a relation as highly likely if (1) the spectral coherence between this response and the 27-day forcing is high (squared coherence between 0.7 and 1) and (2) the frequency dependence of the phase spectrum is smooth in the close neighborhood of the 27-day period. See Sect. 5.4. for the discussion of spectral coherences and Sect. 5.6 to 5.8 for the discussion of phase lags computed by this method.

4 Analysis of the 27-day variation in solar irradiance data

In order to establish the amplitude A_λ of the idealized 27-day solar forcing, we analyzed the spectral solar fluxes kindly provided by Judith Lean, Naval Research Laboratories,

USA, in the range 120.5–739.5 nm. The data consist of daily mean values with a spectral resolution of 1 nm for the period 1990–2000 (Lean et al., 1997, 2000) derived from measurements made by the Solar Stellar Irradiance Comparison Experiment (SOLSTICE) onboard the Upper Atmosphere Research Satellite (UARS). A power spectrum analysis over the 11-year period reveals a strong signal with a mean period of about 26.5 days. The second harmonic is weaker than the main harmonic by a factor of 5–10 (depending on the time period and the spectral range considered), while higher harmonics are negligible.

Figure 1a shows the time-dependent spectral density of the solar 205 nm flux. Significant variations in the amplitude of near-27-day variability can be identified. The spectral density corresponding to the solar activity maximum near 1990 is larger by a factor of 4 than the density for the following solar maximum near 2000, resulting in an amplitude ratio of 2 to 1. The amplitudes during solar minimum (~1995–1997) are approximately an order of magnitude smaller than during the 1990 solar maximum. The period of this solar variation also changes slightly with time.

To calculate the amplitudes and phases of the 27-day cycle and its harmonics we choose the period January to June 1990. Figure 1a shows that the period of the solar variation increases during this period. Amplitudes and phases of the 27-day and higher harmonics have been calculated by a harmonic analysis (decomposition into discrete Fourier row). The amplitudes of the 27-day and 13.5-day harmonics for the period January to June 1990 are shown in Fig. 1b. In the model simulations, we use the 27-day oscillation amplitudes calculated for this half-year period as amplitudes A_λ for our idealized 27-day solar forcing. Higher harmonics are neglected.

5 Model results and their discussion

Unlike 1-D and 2-D models, HAMMONIA produces internal variability in dynamical variables that cover a broad spectral range. This variability on the one hand should lead to more realistic results. On the other hand it significantly complicates the analysis of

27-day solar signals since internal atmospheric disturbances may have periods close to the forcing. In this section we begin the analysis by methods that are commonly used for this kind of study. However, later we present a combination of spectral methods that allows not only to detect 27-day signals, but also to assess the relation of these signals to the solar forcing.

All model data used for the analysis are daily and zonally averaged.

5.1 Correlations of 27-day variations in tropical ozone and temperature with the solar forcing

One can suppose that, if the 27-day solar forcing produces any response in the atmosphere, this response should be coherent with the forcing for a sufficiently long time (i.e., during several 27-day cycles). A frequently applied way to assess the relation between atmospheric short-term variations and the 27-day solar forcing is to derive the correlations between atmospheric and solar variations. Therefore, we extract the near-27-day variations in several atmospheric model parameters with a combination of two Kaiser-Bessel filters, and then calculate the correlation coefficients between the filtered time series and the solar forcing for different time lags. Figure 2a and b show the corresponding correlation coefficients as a function of altitude and the time lag for tropical (averaged over 20° S–20° N) ozone and temperature variations calculated for the entire 5-year period of simulation S27.

The maximum value of the correlation coefficient for ozone is about 0.5 at 35 km (Fig. 2a). This is within the range of maximum correlation coefficients reported for ozone at a similar altitude in the observational studies by Hood (1986), Hood and Cantrell (1988), Fleming et al. (1995), and Hood and Zhou (1998). It is slightly smaller than the maximum correlation coefficients obtained in the (2-D and 3-D) model studies by Fleming et al. (1995), Williams et al. (2001), and Zhu et al. (2003). However, the magnitude of these correlation coefficients depends crucially on the type of filtering applied to the original time series. With respect to the phase of the signal, there is a good correspondence between our results presented in Fig. 2a and the results of satellite

ozone data analysis by Fleming et al. (1995, Fig. 1) and by Zhou et al. (1997, Fig. 7). The three figures exhibit similar phase shifts with altitude in the stratosphere and a secondary maximum in the mesosphere that is in an opposite phase to the forcing. However, while this maximum occurs at about 65 to 70 km in Fleming et al. (1995) and in our study, it is closer to 50 km in the study by Zhou et al. (1997). A more detailed comparison with observations can be found in Sect. 5.8.

The stratospheric ozone response is explained e.g. by Brasseur et al. (1987) as a combined effect of the increased photodissociation of O_2 for increased UV irradiance and the temperature dependence of ozone production and loss rates. The negative effect in the mesosphere is caused by the increased OH production via the photodissociation of water vapor by Lyman-α radiation (e.g. Brasseur et al., 1993). The negative response that occurs in our simulations in the mesopause region and above is due to the photodissociation of ozone and the temperature dependence of its production. The negative response around the mesopause is in contrast to a positive response observed in the simulations of the 11-year cycle effect with the same model (Schmidt et al., 2006). Apparently, the effect of downward molecular diffusion of atmospheric oxygen produced by stronger O_2-photodissociation in the thermosphere is of less importance on the 27-day time scale.

The maximum of the temperature correlation coefficient of about 0.3 close to the stratopause (~50 km) in Fig. 2b and its position are in rather good agreement with studies of Hood (1986), Hood and Cantrell (1988), and Hood and Zhou (1998). The temperature response is a direct effect of increased UV irradiance combined with stronger absorption by the increased ozone concentration in the stratosphere.

The results of the correlation analysis suggest that the simulated ozone and temperature signals in the middle and upper atmosphere are closely related to the 27-day solar forcing. However, they provide no proof. Application of the same technique to ozone and temperature data obtained in the simulation that does not include a 27-day forcing (S0, Fig. 2c and d) yields coefficients that are in some regions of similar magnitude as the coefficients derived from S27. Due to the significant length of the time

series, all correlation coefficients derived from simulations S0 and S27 in Fig. 2 are statistically significant. This result calls for the application of more sophisticated analysis methods.

5.2 Wavelet transform analysis

Another problem of analyzing the atmospheric response to the 27-day solar forcing is the possibility of intrinsic atmospheric variations with periods close to the periode of forcing. Figure 3 shows results of a wavelet analysis of ozone concentrations at 40 km and 90 km altitude at 50° N for the S27 and S0 simulations, respectively. Figure 3a and 3b show that variations with a period of 27 days are accompanied by variations with other periods (in particular in the disturbed winter stratosphere). Moreover, there is significant interannual variability of the signals with periods close to 27 days. Note e.g. the weaker signal during the first than during the second summer in Fig. 3a. Figure 3c and d show that ozone variations with periods close to 27 days can occur (again in particular in the winter stratosphere) also in the case without solar forcing. At both altitudes the variability on a time scale close to 27 days is increased in the simulation with solar forcing. But it seems impossible to clearly distinguish internal and forced variability with this filtering technique.

The reason of this problem is the relatively poor spectral resolution of any filter. A filtered variation with fixed period may be related to variations within a more or less broad band around this exact period.

5.3 Spectral analysis

The previous sections have shown that filter and correlation techniques do not provide an adequate method to analyze the atmospheric response to 27-day solar forcing. Other methods are needed, which can provide a better spectral resolution. In the following, high-resolution spectral and cross-spectral analysis methods are applied.

Figures 4a–d show the results of a spectral-time analysis of ozone mixing ratios for

the altitudes of 35 and 100 km at the equator and 50° N for the simulation S27, while Fig. 4e and f show results for 50° N from the simulation without 27-day forcing (S0). Figure 4a–d exhibit distinctive 27-day signals in the middle stratosphere and in the mesopause layer. There is no repeated 27-day signal in ozone in the case without forcing, although the spectral analysis reveals variations with periods close to 27 days, for example in winters 3 and 4 at 35 km, and in winters 3 and 5 at 100 km. A striking feature of the 27-day signal in Fig. 4a–d is its intermittent character. There is significant seasonal and interannual variability of the 27-day signal in both mid-latitudes and tropics. Since the amplitude of the applied 27-day forcing is constant with time the 27-day ozone signal is probably influenced by internal atmospheric dynamics. One intriguing feature in the simulations at 50° N is the presence of strong wintertime oscillations with periods between 16 and 20 days in the case without forcing (Fig. 4e and f). These appear much less prominent when the forcing is introduced. Theoretically, two explanations can be provided: a) The 27-day forcing affects an inherent state of the atmosphere, and its free oscillation properties change. b) The response to the 27-day forcing can interact nonlinearly with intrinsic atmospheric oscillations, generating oscillations at combination frequencies. A combined variation with a period close to 16–20 days but out of phase with the original variation may attenuate it. It is difficult to establish which hypothesis is more likely. However, non-linear interactions of the 27-day signal with other intrinsic atmospheric variations may explain the intermittent character of the model response to the 27-day forcing. According, e.g. to Chandra (1985), and Ebel et al. (1988), the atmospheric response to 27-day forcing is presumably modified by stationary and transient planetary waves which are of a very intermittent character themselves.

Figure 5 shows altitude profiles of ozone power spectra at the equator and 50° N averaged over four three-month periods of December–February and five three-month periods of June–August, respectively. As it might be expected the equatorial responses in winter and summer are similar. In the mid-latitude stratosphere, the signal is easier to identify in summer, when the intrinsic variability is significantly smaller than in winter.

As in Fig. 4, strong variations are not only identifiable at exactly 27 days but also at very close periods. At 50N and at about 40 km, e.g., two distinct maxima appear in the power spectrum at frequencies slightly longer and shorter than 27 days. Ebel et al. (1981) have suggested that an amplitude modulation with semi-annual or annual periods may lead to such a shift of the original 27-day signal. Although it is very likely that the strong features with periods close to 27 days are indicative of a response to the solar variability our analysis method provides no proof for this assumption. This difficulty is underlined by the spectra for the case without forcing (see Fig. 4 for running spectra, seasonal spectra not shown) that indicate some power for internal variability with periods close to 27 days.

5.4 Spectral coherence analysis

We conclude from the previous section that the spectral analysis itself does not distinguish between the response to 27-day solar forcing and intrinsic atmospheric variations with close periods. However, atmospheric variations related to the 27-day solar forcing should be coherent with the forcing over long time periods. This cannot be expected for intrinsic variations. High values of spectral coherence at periods close to 27 days should thus be a clear indication for a solar forcing effect.

Figure 6 shows altitude-dependent squared coherence spectra obtained for ozone and temperature at the equator and at 50° N, respectively. In the thermosphere the squared coherence at period of about 27 days has high values for ozone and temperature. In the mesosphere and stratosphere, however, the coherence for ozone decreases, particularly at 50° N latitude, while relatively high values remain in some layers over the equator. Coherence values for temperature drop dramatically below 105 km. This difference between ozone and temperature corresponds to different values of the correlation coefficients in Fig. 2. In the case of ozone, no coherence is observed below 30 km while, in the case of temperature, two areas of non-zero coherence are derived for the lower stratosphere (50° N) and the lower troposphere (equator), respectively.

Note that the coherence spectra are derived here for the entire simulation period of

5 years. Seasonally calculated coherence spectra are not meaningful. First, to provide sufficient spectral resolution, a cross-spectral analysis requires longer time series than spectral analysis (see e.g. Jones, 1978). Second, a season contains only three 27-day cycles, and three variations with a period close to 27 days may be coherent with the solar variation (with arbitrary phase lag) even without being related to the forcing.

Altitude-latitude distributions of squared coherence between ozone and temperature, respectively, and the 27-day solar forcing are shown in Fig. 7a–d for two cases: with standard (S27) and with enhanced (S27*3) forcing. The cross-spectral analysis was performed for each altitude and each latitude of the model grid. The spectral coherence is plotted if the coherence maximum is found within the 26–28 day period range. If there is no coherence maximum in this range the coherence value is set to zero. Shown in Fig. 7 are only areas with squared coherence larger than 0.5. The strengthening of the 27-day forcing by a factor of 3 significantly increases the coherence of the response in the upper stratosphere and lower mesosphere, especially in the case of temperature. The coherence is generally low below 30–40 km and close to 70 km. In the case of standard forcing, the squared coherence values are large (higher than 0.7) in the thermosphere (above 100–105 km) at all latitudes in the case of temperature and above 80 km at all non-polar latitudes in the case of ozone. For enhanced solar forcing, the ozone and temperature responses are also highly coherent with the forcing in the upper stratosphere and lower mesosphere. In the case of temperature, this is limited to tropical and mid-latitudes while it extends to very high latitudes in the case of ozone.

A comparison of the spectral coherences in Fig. 7a and b with the correlation coefficients in Fig. 2a and b reveals that e.g. in the case of ozone at altitudes below 30 km non-zero correlations can be calculated in regions of incoherent signals.

5.5 Sensitivity of the response to the 27-day solar forcing

Since the magnitude of the real 27-day solar forcing changes with time and since observational studies cover different time periods, the sensitivity of the response to the 27-day solar forcing is a more convenient quantity than the amplitude. Here, this sensi-

tivity is defined as the change in e.g. ozone or temperature per 1% change of the solar 205 nm radiation.

In Figs. 8–10 we present seasonally dependent altitude-latitude distributions of response sensitivities estimated from spectral analysis. If a spectral estimate is statistically insignificant or if the coherence value obtained from cross-spectral analysis is less than a threshold value the sensitivity is not plotted. Since seasonal coherence values are not available, coherences calculated for the whole period of the simulation were used. The threshold value for squared coherence is chosen to be equal to 0.5 for the case of standard 27-day solar forcing (S27) and to 0.7 for the case of enhanced forcing (S27*3).

Figures 8 and 9 show December–February and June–August sensitivities of ozone and temperature, respectively, to the standard and enhanced 27-day solar forcing. The strongest ozone sensitivity of more than 10% is characteristic for the thermosphere. Local altitude maxima of the sensitivity are noted in the upper mesosphere and in the upper stratosphere. It is worth to note the nonlinearity of the ozone response, especially for layers in the neighborhood of 40 and 80 km where the sensitivity decreases with increasing forcing. Over the tropics the ozone sensitivity in the upper stratosphere is about 0.5–0.6% for the standard forcing case and about 0.3% for the case of enhanced forcing.

Figure 8 exhibits that in the thermosphere the sensitivity of the ozone response is larger during winter than during summer. This seems to be also the case around the stratopause. However, the criteria of statistical significance and high coherence are not met everywhere at these altitudes.

The sensitivity of the temperature response has no significant seasonal dependence in the thermosphere (Fig. 9). In the upper mesosphere, the strongest mid-latitude response seems to occur in summer while in the upper stratosphere it occurs during winter (Fig. 9c and d). This latter feature corresponds well to the winter extratropical maximum of ozone sensitivity in the same layer shown in Fig. 8. As for the ozone response, the temperature response is nonlinear. In the lower mesosphere, the maxi-

mum temperature sensitivity at the equator is about 0.4 K for the standard forcing, while it is only of the order of 0.15 K for the case of the enhanced forcing.

Similar non-linearities occur in the responses of other chemical species. Figure 10 shows sensitivities of $O(^3P)$, water vapor, OH, NO, NO_2, and HNO_3 for December–February in the case of the enhanced forcing (since for this case results are available for larger areas).

Atomic oxygen (Fig. 10a) has its maximum response of about 1% in the upper mesosphere. Unlike for ozone, the $O(^3P)$ sensitivity decreases with altitude in the thermosphere.

Water vapor is dissociated through short wave UV (Lyman-α). Its response to the 27-day solar forcing is reliably detected only above 75 km (Fig. 10b) where the water vapor content is relatively small. The water vapor response in the extratropical latitudes is seasonally dependent above approximately 90 km, with a maximum sensitivity in the summer hemisphere.

Atmospheric hydroxyl, which is produced in the mesosphere and thermosphere as a product of the water vapor photolysis, has response maxima of about 1% in the upper mesosphere-lower thermosphere (Fig. 10c). Since the vertical distribution of OH has a maximum in the upper mesosphere, the large amplitude in the OH response during summer may be identifiable in ground-based observations of hydroxyl emissions.

Nitric oxide has its absolute maximum response of about 2% between 90 and 100 km in the summer hemisphere (Fig. 10d), where the nitric dioxide response has a weak local maximum (Fig. 10e). The absolute maximum of the NO_2 sensitivity occurs at about 85 km altitude and is probably related to the reaction with OH. The stratospheric maxima in NO and NO_2 sensitivities (about 0.4%) are observed in the layer of maximum NO_2 concentration near 30 km altitude and may thus be identifiable by column NO_2 measurements.

An interesting feature in the nitric acid response is a mid-latitude winter maximum of about 2% in the upper stratosphere-stratopause layer (Fig. 10f). The same feature is observed in the southern hemisphere winter. These sensitivity maxima occur at the

same location as the maxima in ozone (Fig. 8a and c) and temperature (Fig. 9c). An absolute maximum of the HNO_3 sensitivity of 3% is noticed in the upper mesosphere layer where the HNO_3 concentration is very small. It corresponds to a similar maximum in NO_2.

5.6 Phase characteristics of the response

The phase characteristics of the atmospheric 27-day signals presented here are obtained from phase spectra for the simulation with enhanced forcing (S27*3). They are similar to characteristics for the S27 simulation but available for larger areas. Like spectral coherence, phase characteristics have been calculated as an average over the whole simulation period. This explains differences between the coverage of phase and sensitivity patterns.

Figure 11 shows altitude-latitude distributions of the time lags of 27-day variations for temperature and for the chemical species treated in the previous section, relative to the solar forcing. In general, the annual mean phase lags exhibit only weak latitude dependence. In the case of ozone, only the mesopause region (90–100 km) is characterized by a peculiar time regime. In low and mid-latitudes, ozone leads the radiation variation by 10 to 12 days, while in the polar region this lead is closer to 6 to 8 days. These polar regions correspond to areas of a high ozone sensitivity shown in Fig. 8c and d. However, to understand this feature, an analysis of the phase's seasonal dependence would be necessary. A phase flip at mid-latitudes as observed by Ruzmaikin et al. (2007) is not clearly identifiable in our results.

Atomic oxygen is produced mainly by photolysis of ozone in the stratosphere and lower mesosphere and by the photolysis of molecular oxygen at higher altitudes. An interesting feature of the atomic oxygen response in the upper stratosphere and lower mesosphere is a latitude gradient of the response phase that changes from a lead in the NH to a lag in the SH (Fig. 11c). The $O(^3P)$ response above 75 km lags behind the solar cycle, and is approximately a quarter-period out of phase with the cycle in the neighborhood of the mesopause where the 27-day variations of atomic oxygen and

ACPD
8, 1113–1158, 2008

EGU

temperature are approximately in phase with each other (cf. Fig. 11b). As it may be expected, the $O(^3P)$ response above 85 km is approximately in opposite phase with the response of molecular oxygen.

The water vapor response above 70 km leads the solar forcing by 6 to 11 days, depending on altitude (Fig. 11d). In the mesopause layer, H_2O variations are almost in opposite phase to the solar variation.

The hydroxyl response in the mesosphere and upper stratosphere is typically in phase with the 27-day solar forcing (Fig. 11e), which is explained by the fact that water vapor photolysis is a major source of OH at these altitudes. In the mesopause layer, OH variations lead solar oscillations by 3–4 days. Above this level, phases of the OH response change abruptly with altitude. Very different responses of OH at different altitudes to solar forcing have also been observed in the 11-year solar cycle numerical experiments (Schmidt et al., 2006). This was attributed to the fact the OH chemistry involves very different chemical reactions with different temperature dependencies that vary substantially with altitude.

Figure 11f exhibits a vertical gradient of the phase of the NO response in the mesosphere and lower thermosphere. The NO phase changes from about a quarter-period lead relative to the solar forcing at 60 km through being in opposite phase at 100 km to a quarter-period lag at 120 km. A strong vertical gradient of the phase of the NO response is also derived for the stratospheric heights of 25–35 km. This vertical structure in the NO phase reflects a variety of processes influencing the NO balance in different parts of the atmosphere, among which are N_2 and NO photolysis in the upper atmosphere, HO_x-NO_x chemistry in the mesosphere, and NO_2 photolysis and ozone photochemistry in the stratosphere.

The altitude structure of the phase of the NO_2 response is simpler than that of NO (Fig. 11g). In the stratosphere, the NO_2 response is almost in phase with the 27-day solar variation. Figure 11h shows that changes in HNO_3 (that are approximately out of phase with NO_2 changes in this layer) may be responsible for the phase of the stratospheric NO_2 response (via photolysis of HNO_3). In the thermosphere, NO_2

ACPD
8, 1113–1158, 2008

EGU

variations are approximately out of phase with the solar forcing. This is probably due to fast photolysis of NO_2. In the upper mesosphere, where hydroxyl is highly sensitive to the 27-day solar forcing (see Fig. 10c) and in phase with it (Fig. 11e), NO_2 variations lead the solar oscillations by up to a quarter-period.

Figure 11h shows that increase in short-wave solar radiation during the 27-day cycle results in a decrease in stratospheric HNO_3 due to photodissociation (with a response lag of 1–2 days). In the upper mesosphere, the phase of the HNO_3 response is close to the phase of the NO_2 response.

5.7 Comparison of results from spectral and linear regression analysis

It is useful to compare sensitivities of ozone and temperature responses to the 27-day solar forcing obtained from spectral analysis with results obtained from linear regression analysis, since in most previous studies only the latter approach was used. Figure 12 shows the altitude distribution of ozone and temperature sensitivities for the tropical belt (20° S–20° N) estimated by the two methods. Note that Fig. 12b uses other units for temperature sensitivity than Fig. 9 (%/% instead of K/%) in order to allow a comparison with observed values. Shown in Fig. 12 are the results obtained by the linear regression method for all three different forcing amplitudes (S0, S27, S27*3). In the first case, the response sensitivities were obtained assuming a fictitious 27-day forcing as in simulation S27.

Below 100 km, the linear regression ozone and temperature sensitivities for the case of enhanced forcing are close to those for the case of standard forcing, suggesting an approximate linearity of the responses. In contrast, spectral estimates of the sensitivities suggest a nonlinearity in the responses. In the case of enhanced forcing, the linear regression and spectral estimates agree well below 70 km altitude. However, we believe that this correspondence is fortuitous and does not point to a deficiency of the spectral estimates for the standard forcing. There is less agreement above 70 km where the spectral coherence with the forcing is larger (cf. Fig. 7a). Moreover, above approximately 110 km where the ozone and temperature responses are more promi-

nent and less disturbed by intrinsic variability (cf. Fig. 2), spectral and linear regression estimates group according to the magnitude of the forcing, and both methods exhibit a nonlinear response (not shown in Fig. 12).

The difference between spectral and linear regression estimates of the sensitivities shown in Fig. 12 is attributed to several causes. First, the definitions are different. In the case of spectral estimates, the sensitivity is calculated based on the amplitude of the response (see Sects. 3 and 5.5). In the case of linear regression estimates, deviations of all magnitudes contribute to the regression. Thus, these estimates are affected by small-magnitude (and, probably, statistically less significant) variations. The latter point is underlined by the small correlation coefficients in Fig. 2. In the upper atmosphere with clearer atmospheric response, linear regression estimates are only slightly larger than spectral estimates. The second and probably more important reason for the difference between the spectral and linear regression sensitivity estimates is the difference in the spectral range of the responses considered by the two methods. The spectral estimates are related only to a response occurring within a relatively narrow frequency range around the forcing period of 27 days. In contrast, the linear regression analysis (even combined with band-pass filtering) involves variations from a much broader frequency range not always associated with the actual solar forcing.

Figure 12 shows that the linear regression technique can provide a response even in the case without applied 27-day solar forcing. The sensitivity of this "response" is in some regions of the atmosphere comparable to the magnitude of the real response. It is worth to note that, unlike the regression method, spectral analysis usually provides sensitivity estimates only for altitudes where the real response is larger than the fictitious response. The criteria of spectral coherence and phase spectrum (see Sect. 3) impose further limitations on the altitude range of reliably detected response. For example, with these criteria it is not possible to relate the 27-day variations from the troposphere to the middle stratosphere (Fig. 12) with the solar forcing.

Figure 13 compares altitude distributions of the phase lags of 20° S–20° N ozone and temperature responses to standard (thin color curves) and enhanced (thick color

ACPD
8, 1113–1158, 2008

EGU

curves) 27-day solar forcing, as estimated by cross-spectral analysis (red curves) and by linear correlation analysis (green curves). Black curves correspond to the lags of the fictitious "response" obtained by the correlation method for the case without 27-day forcing. The lags derived by the two methods are in very good agreement above 120 km (not shown in Fig. 13). Below 120 km there are systematic differences between lag values derived by the different methods as well as between lag values derived by cross-spectral analysis for the cases of standard and enhanced solar forcing. According to results of cross-spectral analysis, ozone in the upper stratosphere responds to the 27-day solar variation (simulation S27) 2–3 days earlier than when it is derived from linear correlation analysis. The phase difference is generally less for the enhanced forcing.

Figure 13b shows that, according to results of cross-spectral analysis, the thermal response to the 27-day solar forcing (of standard amplitude) occurs in the upper stratosphere and around the mesopause 2–3 days earlier than calculated with the linear correlation method.

5.8 Comparison with observations

In addition to model results, Figs. 12 and 13 present sensitivities and phase lags of ozone and temperature responses derived in different observational studies. The majority of these sensitivity and lag estimates was obtained by the linear regression method. Horizontal error bars in Fig. 12 are standard deviations from the mean observed values.

The spread of the experimental results is in general larger for temperature than for ozone. Figure 12a shows that in the 30–65 km layer the ozone sensitivities derived from our model calculations are within the broad range of values suggested by observations. Modeling and observations reveal that the maximum ozone sensitivity is located in the upper stratosphere close to 40 km. However, above 65 km, the agreement between the model and observational ozone sensitivities is less satisfactory. Around 70 km altitude, observations exhibit high ozone sensitivity (of the order of 0.5%) while the spectral analysis of model results does not provide reliable sensitivity estimates. This is due

to the low coherence between response and forcing (see Fig. 7a and c). Above about 75 km, the simulated ozone sensitivity is stronger than suggested by observations.

There is a good agreement between model and experimental estimates of the temperature sensitivity in the neighborhood of the stratopause (Fig. 12b). Below this region, our simulated sensitivities are smaller than the observed ones. In the neighborhood of the mesopause layer, our simulation and the only observational study available exhibit principal differences not only in the magnitude of temperature response but also in its altitude dependence. However, the temperature sensitivity estimates suggested in this experimental study (Hood et al., 1991) for lower altitudes differ significantly from other experimental studies (see Fig. 12b). It is worth to note the large discrepancy of different experimental estimates of the temperature response in the mid mesosphere, i.e. just in the layer where, according to the linear regression analysis of model results, the amplitude of the fictitious temperature response for the simulation without forcing exceeds the amplitude calculated with the forcing.

As for the sensitivity, there is a satisfactory agreement between model and experimental estimates of the phase of the ozone response and its altitude dependence in the upper stratosphere (Fig. 13a). In the lowermost mesosphere, different experimental studies provide different phase lags. The observed altitude dependence above 60 km is more complicated than the simulated one. In the model, the only sharp phase change (from in phase below to out of phase above) occurs around 65–70 km, while the phase of the observed ozone response undergoes twice a sharp change by about half a period at approximately 60 and 75 km altitude, respectively. The lower phase change corresponds qualitatively to the similar change in modeled ozone response (occurring slightly higher). The second phase jump is not reproduced by the model. However, both observational studies for this altitude range are based on data from the same Solar Mesosphere Explorer (SME) instrument (Keating et al., 1987; Hood et al., 1991).

One can distinguish between two groups of experimental results concerning the phase of the temperature response (Fig. 13b). One group (smaller) provides a tem-

perature response lag close to zero or small positive values. Another group (larger) exhibits a significant altitude dependence of the phase with a lag in the middle stratosphere and a lead in the upper mesosphere. In the upper stratosphere, there is a good correspondence between the model cross-spectral estimates of temperature response lag and the lag values suggested by the minority group of observations. In the lower mesosphere, the model estimates are still within the broad range of the lag values suggested by observational studies. However, above 75 km, there is a significant discrepancy between the model cross-spectral estimates and the results of the only observational study available for this altitude (Hood et al., 1991). It is interesting to note the similarity in the altitude dependence of temperature response phases suggested by the major group of observations and the phase of the fictitious temperature response derived from model calculations without 27-day solar forcing (black curve in Fig. 13b)

To our knowledge, the only study of chemical parameters other than ozone is provided by Keating et al. (1986) who analyzed 27-day variations in stratospheric HNO_3 and NO_2 using the Nimbus 7 LIMS measurements. These authors found that NO_2 and HNO_3 concentrations at 10 hPa (~30 km) correlate and anti-correlate, respectively, with 27-day UV solar variations. These results are in qualitative agreement with results from our model (see Fig. 11g and h).

5.9 The dynamical response to solar 27-day forcing

Some features of the calculated response may be difficult to explain invoking only photochemical and radiative mechanisms, and not taking into account the possible role of dynamical processes. For example, the enhanced sensitivity of the stratospheric ozone response in the middle and high latitudes during wintertime (Fig. 8) points to the likely important role of the circulation (see also Ruzmaikin et al., 2007). Sensitivity maxima for temperature, nitric acid, and ozone are derived for the same location (compare Figs. 8a, 9c and 10f as well as Figs. 8b and 9d), thereby suggesting the existence of a common cause. Furthermore, the amplitudes of this wintertime mid-latitude ozone

response for the enhanced forcing case are similar to the amplitudes derived for the standard forcing case (while the associated sensitivities differ by about a factor of 3, compare Fig. 8a and c as well as Fig. 8b and d). These features might be easier to explain by an effect of the 27-day solar variation on the atmospheric circulation. However, cross-spectral analysis has not revealed near-27-day variations in zonal mean daily mean values of zonal, meridional and vertical wind components coherent with the forcing. One probable reason is that the 27-day effect in circulation is masked under Eulerian and/or diurnal averaging, and another approach is needed for analyzing such effects.

At present, the possible response of the atmospheric dynamics to 27-day solar forcing remains an open question. Dameris et al. (1986) and Ebel et al. (1988), using a three-dimensional mechanistic model, found that the response to a 27- and 13-day solar forcing prescribed at the stratopause may propagate downward depending on the background wind and on the planetary wave distribution. Ivanovskii and Krivolutskii (1979) suggested the possibility of resonant excitation of traveling planetary waves caused by 27-day solar forcing. This was confirmed by Krivolutsky et al. (2003), who derived a resonant response in a hemispheric model atmosphere, and attributed it to a non-zonality of the ozone distribution. Pogoreltsev et al. (2002), however, could not confirm the existence of global free modes in the middle atmosphere with periods close to 27 or 13 days. Luo et al. (2001) have observed wind oscillations of 20–40 day periods in the mesosphere and lower thermosphere and suggested a possible solar origin. All these possible influences can not be confirmed by our analysis.

6 Conclusions

We have presented a first modeling study of the atmospheric effect of the 27-day solar rotational variation, using a 3-dimensional chemistry climate model that covers the atmosphere from the surface to the thermosphere. To analyze the atmospheric response to the 27-day solar forcing, we used a variety of spectral and cross-spectral analysis

techniques, in addition to the linear correlation and regression methods used in most previous observational and modeling studies.

The HAMMONIA model used in this study produces a broad spectrum of internal atmospheric variability including periods close to 27 days. Our analysis has revealed shortcomings of the correlation (and regression) analysis method. Apparent signals derived by this method may not be a response to the solar forcing but just represent a part of the internal atmospheric variability. The combination of high resolution spectral and cross-spectral methods allows identifying 27-day variations in the atmosphere which are actually related to the solar forcing. These methods can also be used to estimate the amplitude and the phase of the response.

Our analysis shows that, while the calculated thermal and chemical responses are very distinct and permanent in the upper atmosphere, the responses in the stratosphere and mesosphere are intermittent and depend probably on the dynamical state of the atmosphere. By analyzing a somewhat different set of 3-D numerical experiments, Rozanov et al. (2006) came to a similar conclusion in particular for the stratospheric temperature response. In an observational study, Ruzmaikin et al. (2007) have suggested the possibility of phase drifts in the stratospheric ozone response that may also lead to the intermittent appearance of signals.

In the extratropical latitudes, the responses are, in general, seasonally dependent. The sensitivity is in many cases stronger in winter than in summer. This has also been observed, e.g. by Ruzmaikin et al. (2007) and is a hint to a possible dynamical response to 27-day solar forcing. To clearly identify such a response, further analysis is needed.

Experiments with different forcing amplitudes have shown that the responses of temperature and of the concentrations of chemical species to 27-day forcing are non-linear. Their sensitivities generally decrease when the forcing increases. This conclusion is important to understand the possible differences of observational studies obtained at times of different forcing amplitudes.

The sensitivity and phase of the ozone response in the tropical stratosphere and

lower mesosphere are in satisfactory agreement with available observational results, while above ~75 km significant differences with observational data exist. However, the number of available observations in this region is low. The simulated sensitivities for the stratospheric temperature response are at the lower edge of the range suggested by observations. The few mesospheric observational studies do not provide a coherent picture of sensitivities. In the case of the phase of the temperature response, it is interesting to note that a fictitious response analyzed for a simulation without forcing indicates a similar shift with altitudes as it was calculated from observations. An important deduction from these findings is that for most atmospheric parameters, at present, there is insufficient observational data for a comprehensive evaluation of simulated 27-day solar forcing effects. The analysis of observational data should include not only periods with a significant amplitude of the 27-day solar variation, but also periods when this forcing is absent or relatively weak. This would provide information about the inherent variability of the atmosphere and thereby help to identify which part of the variability is related to the solar forcing. It is also important that the analysis of observed and simulated data be made by the same method.

In addition to ozone, our simulations show effects of 27-day solar forcing on other chemical species. Some of these responses should be identifiable in existing observations, for example in the measurements of stratospheric nitrogen oxides or of mesospheric OH.

Acknowledgements. We thank J. Lean for providing the spectral solar fluxes and V. A. Bezverkhny for providing the code used to perform the high resolution spectral analysis. The work was partly financed by the CAWSES priority program of the Deutsche Forschungsgemeinschaft (DFG). One of the authors (A .N. Gruzdev) was also financially supported by the Russian Foundation for Basic Research within the projects No 05-05-65034 and 08-05-00358, by the Program No 16 of the Presidium of the Russian Academy of Sciences, and by the grant of the President of Russia for scientific schools No 4166.2006.5. The numerical simulations were performed at the German Climate Computing Centre (DKRZ).

References

Bezverkhny, V. A.: Spectral analysis of short observational series (in Russian), preprint of the Institute of Atmospheric Physics, Moscow, 1986.

Brasseur, G.: The response of the middle atmosphere to long-term and short-term solar variability: A two-dimensional model, J. Geophys. Res., 98, 23 079–23 090, 1993.

Brasseur, G., De Rudder, A., Keating, G. M., and Pitts, M. C.: Response of middle atmosphere to short-term solar ultraviolet variations: 2. Theory, J. Geophys. Res., 92, 903–914, 1987.

Chandra, S.: Solar-induced oscillations in the stratosphere: A myth or reality?, J. Geophys. Res., 90, 2331–2339, 1985.

Chandra, S., McPeters, R. D., Planet, W., and Nagatani, R. M.: The 27-day solar UV response of stratospheric ozone: Solar cycle 21 versus solar cycle 22, J. Atmos. Terr. Phys., 56, 1057–1065, 1994.

Chen, L., London, J., and Brasseur, G.: Middle atmosphere ozone and temperature responses to solar irradiance variations over 27-day periods, J. Geophys. Res., 102, 29 957–29 979, 1997.

Dameris, M., Ebel A., and Jakobs, H. J.: Three-dimensional simulation of quasi-periodic perturbation attributed to solar activity effects in the middle atmosphere, Ann. Geophys., 4A, 287–296, 1986.

Ebel, A., Schwister, B., and Labitzke, K.: Planetary waves and solar activity in the stratosphere between 50 and 10 mbar, J. Geophys. Res., 86, 9729–9738, 1981.

Ebel, A., Dameris, M., and Jakobs, H. J.: Modeling of the dynamical response of the middle atmosphere to weak external forcing: Influence of stationary and transient waves, Ann. Geophys., 6A, 501–512, 1988.

Eckman, R. S.: Response of ozone to short-term variations in the solar ultraviolet radiance. 1. A theoretical model, J. Geophys. Res., 91, 6695–6704, 1986a.

Eckman, R. S.: Response of ozone to short-term variations in the solar ultraviolet radiance. 2. Observations and interpretation, J. Geophys. Res., 91, 6705–6721, 1986b.

Fleming, E. L., Chandra, V., Jackman, C. H., Considine, D. B., and Douglass, A. R.: The middle atmosphere response to short and long term UV variations: Analysis of observations and 2D model results, J. Atmos. Terr. Phys., 57, 333–365, 1995.

Gille, J. C., Smyth, C. M., and Heath, D. F.: Observed ozone response to variations in solar ultraviolet radiation, Science, 225, 315–317, 1984.

Giorgetta, M. A., Manzini, E., Roeckner, E., Esch, M., and Bengtsson, L.: Climatology and Forcing of the QBO in MAECHAM5, J. Climate, 19, 3882–3901, 2006.
Gruzdev, A. N. and Bezverkhny, V. A.: Two regimes in the quasi-biennial variation of the equatorial stratospheric wind, J. Geophys. Res., 105, 29 435–29 443, 2000.
Gruzdev, A. N. and Bezverkhny, V. A. : Quasi-biennial oscillation in the atmosphere over North America from ozonesonde data, Izvestiya, Atmos. Oceanic Phys., 41, 29–42, 2005.
Harris, F. J.: On the use of windows for harmonic analysis with the discrete Fourier transform, Proc. Ieee., 66, 51–83, 1978.
Hood, L. L.: The temporal behavior of upper stratospheric ozone at low latitudes: evidence from Nimbus 4 BUV data for short-term responses to solar ultraviolet variability, J. Geophys. Res., 89, 9557–9568, 1984.
Hood, L. L.: Coupled stratospheric ozone and temperature response to short-term changes in solar ultraviolet flux: Analysis of Nimbus 7 SBUV and SAMS data, J. Geophys. Res., 91, 5264–5276, 1986.
Hood, L. L.: Solar ultraviolet radiation induced variations in the stratosphere and mesosphere, J. Geophys. Res., 92, 876–888, 1987.
Hood, L. L. and Cantrell, V.: Stratospheric ozone and temperature responses to short-term solar ultraviolet radiations: Reproducibility of low-latitude response measurements, Ann. Geophys., 6, 525–530, 1988,
http://www.ann-geophys.net/6/525/1988/.
Hood, L. L. and Zhou, S.: Stratospheric effect of 27-day solar ultraviolet variations: An analysis of UARS MLS ozone and temperature data, J. Geophys. Res., 103, 3629–3638, 1999.
Hood, L. L. and Zhou, S.: Stratospheric effect of 27-day solar ultraviolet variations: The column ozone response and comparison of solar cycles 21 and 22, J. Geophys. Res., 104, 26 473–26 479, 1999.
Hood, L. L., Huang, Z., and Bougher, S. W.: Mesospheric effects of solar ultraviolet variations: Further analysis of SME IR ozone and Nimbus 7 SAMS temperature data, J. Geophys. Res., 96, 12 989–13 002, 1991.
Ivanovskii, A. I. and Krivolutskii, A. A.: Possibility of resonance excitation of large-scale waves, Meteorologiya i Gidrologiya, 6, 97–99, 1979.
Jenkins, G. M. and Watts, D. G.: Spectral Analysis and its Application, San Francisco, Holden-Day, 1968.
Jones, R. H.: Multivariate autoregression estimation using residuals, in: Applied Time Series

Analysis, edited by: Findley, D. F., Academic Press, New York, 139–162, 1978.
Keating, G. M., Brasseur, G. P., Nicholson III, J. Y., and De Rudder, A.: Detection of the response of ozone in the middle atmosphere to short-term solar ultraviolet variations, Geophys. Res. Lett., 12, 449–452, 1985.
Keating, G. M., Nicholson III, J., Brasseur, G., De Rudder, A., Schmaltz, U., and Pitts, M.: Detection of stratospheric HNO_3 and NO_2 response to short-term solar ultraviolet variability, Nature, 322, 43–46, 1986.
Keating, G. M., Pitts, M. C., Brasseur, G., and De Rudder, A.: Response of middle atmosphere to short-term solar ultraviolet variations: 1. Observations, J. Geophys. Res., 92, 889–902, 1987.
Keckhut, P. and Chanin, M. L.: Middle atmosphere response to the 27-day solar rotation as observed by lidar, Geophys. Res. Lett., 19, 809–812, 1992.
Kinnison, D. E., Brasseur, G. P., Walters, S., Garcia, R. R., Marsh, D. R., Sassi, F., Harvey, V. L., Randall, C. E., Emmons, L., Lamarque, J. F., Hess, P., Orlando, J. J., Tie, X. X., Randel, W., Pan, L. L., Gettelman, A., Granier, C., Diehl, T., Niemeier, U., and Simmons, A. J.: Sensitivity of chemical tracers to meteorological parameters in the MOZART-3 chemical transport model, J. Geophys. Res., 112, D20302, doi:10.1029/2006JD007879, 2007.
Krivolutsky, A. A., Kiryushov, V. M., and Vargin, P. N.: Generation of wave motions in the middle atmosphere induced by variations of the solar ultraviolet radiation flux (based on UARS satellite data), Int. J. Geomagn. Aeronom., 3, 267–279, 2003.
Lean, J., Rottman, J., Kyle, G. J., Woods, H. L., Hickey, T. N., and Pugga, J. R.: Detection and parameterization of variations in solar mid and near-ultraviolet radiation (200–400 nm), J. Geophys. Res., 102, 29 939–29 956, 1997.
Lean, J.: Evolution of the Sun's Spectral Irradiance Since the Maunder Minimum, Geophys. Res. Lett., 27, 2425–2428, 2000.
Luo, Y., Manson, A. H., Meek, C. E., Igarashi, K., and Jacobi C.: Extra long period (20–40 day) oscillations in the mesospheric and lower thermospheric winds: observations in Canada, Europe and Japan, and considerations of possible solar influences, J. Sol.-Terr. Phys., 63, 835–852, 2001.
Manzini, E., Giorgetta, M. A., Esch, M., Kornblueh, L., and Roeckner, E.: Sensitivity of the Northern Winter Stratosphere to Sea Surface Temperature Variations: Ensemble Simulations with the MAECHAM5 Model, J. Climate, 19, 3863–3881, 2006.
Offermann, D., Jarisch, M., Schmidt, H., Oberheide, J., Grossmann, K. U., Gusev, O., Russell

III, J. M., and Mlynczak, M. G.: The “wave turbopause”, J. Atm. Sol.-Terr. Phys., 69(17–18), 2139–2158, doi:10.1016/j.jastp.2007.05.012, 2007.

Pogoreltsev, A. I., Fedulina, I. N., Mitchell, N. J., Muller, H. G., Luo, Y., Meek, C. E., and Manson, A. H.: Global free oscillations of the atmosphere and secondary planetary waves in the mesosphere and lower thermosphere region during August/September time conditions, J. Geophys. Res., 107, 4799, doi:10.1029/2001JD001535, 2002.

Roeckner, E., Bäuml, G., Bonaventura, L., Brokopf, R., Esch, M., Giorgetta, M., Hagemann, S., Kirchner, I., Kornblueh, L., Manzini, E., Rhodin, A., Schlese, U., Schulzweida, U., and Tompkins, A.: The atmospheric general circulation model ECHAM 5. Part I: Model description, Technical Report 349, MPI for Meteorology, Hamburg, Germany, 2003.

Roeckner, E., Brokopf, R., Esch, M., Giorgetta, M., Hagemann, S., Kornblueh, L., Manzini, E., Schlese, U., and Schulzweida, U.: Sensitivity of simulated climate to horizontal and vertical resolution in the ECHAM5 atmosphere model, J. Climate, 19, 3771–3791, 2006.

Rozanov, E., Egorova, T., Schmutz, W., and Peter, T.: Simulation of the stratospheric ozone and temperature response to the solar irradiance variability during sun rotation cycle, J. Atm. Sol.-Terr. Phys., 68, 2203–2213, 2006.

Ruzmaikin, A., Santee, M. L., Schwartz, M. J., Froidevaux, L., and Pickett, H. M.: The 27-day variations in stratospheric ozone and temperature: New MLS data, Geophys. Res. Lett., 34, L02819, doi:10.1029/2006GL028419, 2007.

Schmidt, H. and Brasseur, G. P.: The response of the middle atmosphere to solar cycle forcing in the Hamburg Model of the Neutral and Ionized Atmosphere, Space Sci. Rev., 125, 345–356, 2006.

Schmidt, H., Brasseur, G. P., Charron, M., Manzini, E., Giorgetta, M. A., Diehl, T., Fomichev, V. I., Kinnison, D., Marsh, D., and Walters, S.: The HAMMONIA Chemistry climate model: Sensitivity of the mesopause region to the 11-year solar cycle and CO_2 doubling, J. Climate, 19, 3903–3931, 2006.

Summers, M. E., Strobel, D. F., Bevilaqua, R. M., Zhu, X., DeLand, M. T., Allen, M., and Keating, G. M.: A model study of the response of mesospheric ozone to short-term solar ultraviolet flux variations, J. Geophys. Res., 95, 22 523–22 538, 1990.

Williams, V., Austin, J., and Haig, J. D.: Model simulations of the impact of the 27-day solar rotation period on stratospheric ozone and temperature, Adv. Space Res., 27, 1933–1942, 2001.

Zhou, S., Rottman, G. J., and Miller, A. J.: Stratospheric ozone response to short- and

intermediate-term variations in solar UV flux, J. Geophys. Res., 102, 9003–9011, 1997.
Zhou, S., Miller, A. J., and Hood, L. L.: A partial correlation analysis of the stratospheric ozone response to 27-day solar UV variations with temperature effect removed, J. Geophys. Res., 105, 4491–4500, 2000.
Zhu, X., Yee, J.-H., and Talaat, E. R.: Effect of short-term solar ultraviolet flux variability in a coupled model of photochemistry and dynamics, J. Atmos. Sci., 60, 491–509, 2003.

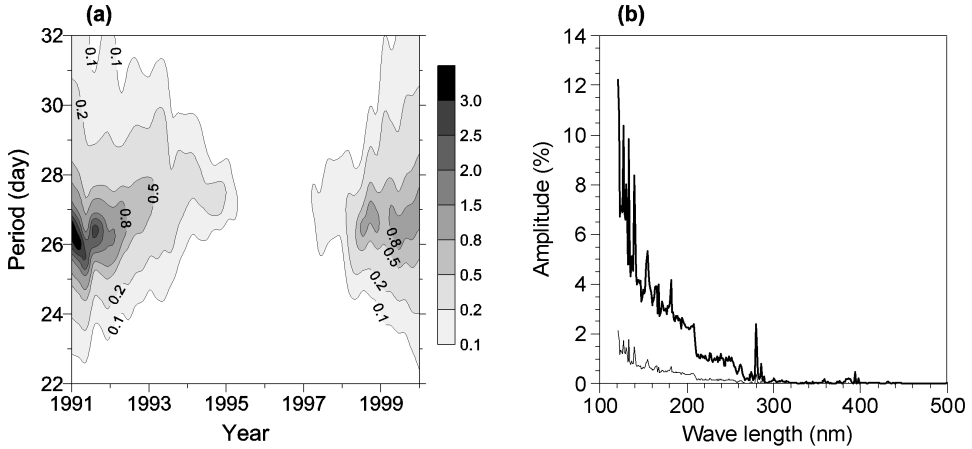

Fig. 1. **(a)** Spectral density of the solar flux at 205 nm as a function of time calculated using 2-year running windows. Units: $(\mathrm{mW/(m^2\,nm)})^2$ day. **(b)** Mean amplitudes of the 27-day (thick curve) and 13.5-day (thin curve) harmonics of the solar extraterrestrial flux as a function of wave length, computed for the period January to June 1990 relative to the mean fluxes for this period.

ACPD
8, 1113–1158, 2008

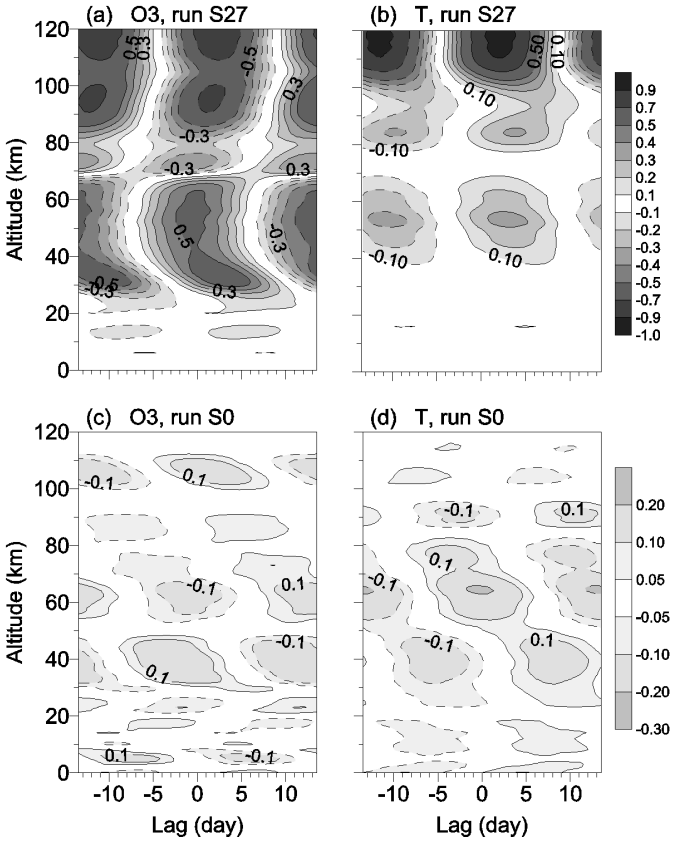

Fig. 2. Correlation coefficients between **(a)** ozone and **(b)** temperature near-27-day variations and the 27-day sinusoidal solar forcing for the tropical belt 20° S–20° N. (a, b) Simulation with applied 27-day forcing, **(c, d)** simulation without 27-day forcing. All shown correlation coefficients are statistically significant at the 95% level.

ACPD
8, 1113–1158, 2008

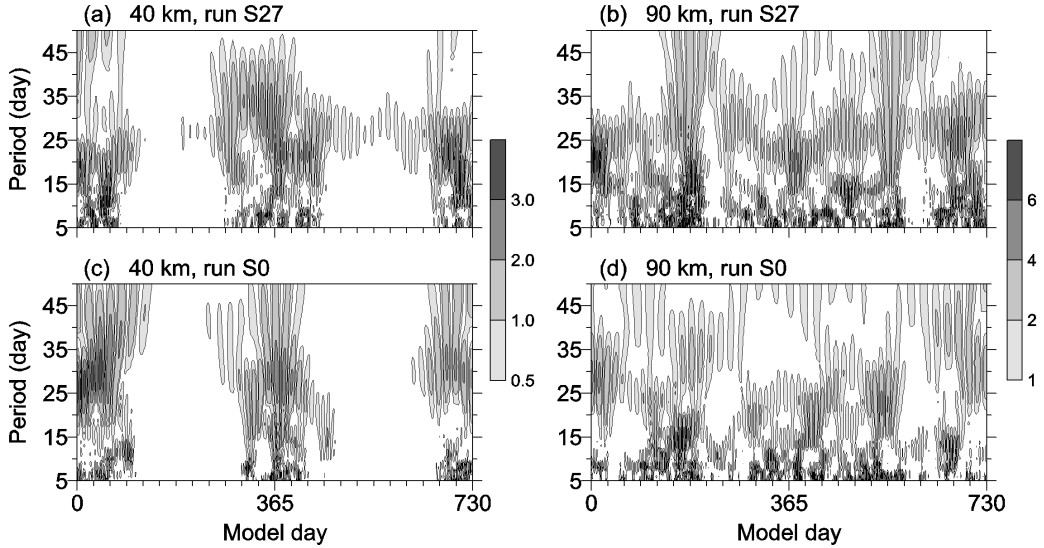

Fig. 3. (a, b) Module of the wavelet transform of the ozone mixing ratios at (a) 40 km and (b) 90 km altitude at 50° N for two model years for the simulation with applied 27-day forcing. **(c, d)** As (a, b) but for the simulation without 27-day forcing. Units: percent of the 5-year mean value.

ACPD
8, 1113–1158, 2008

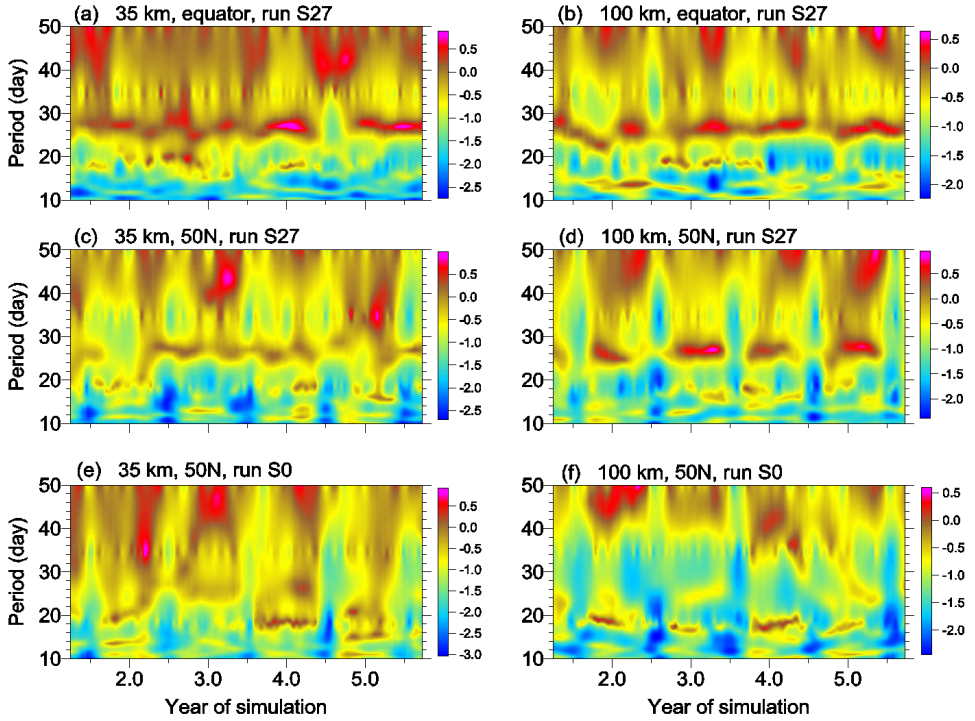

Fig. 4. Logarithm of the spectral density of the ozone mixing ratio as a function of time at **(a)** 35 km and **(b)** 100 km at the equator, at **(c)** 35 km and **(d)** 100 km at 50° N for the case with 27-day forcing, and at **(e)** 35 km and **(f)** 100 km levels at 50° N for the case without 27-day forcing. Units of spectral density: ppmv^2 day. Integer numbers at the horizontal axes correspond to the start of the respective simulated year.

ACPD
8, 1113–1158, 2008

EGU

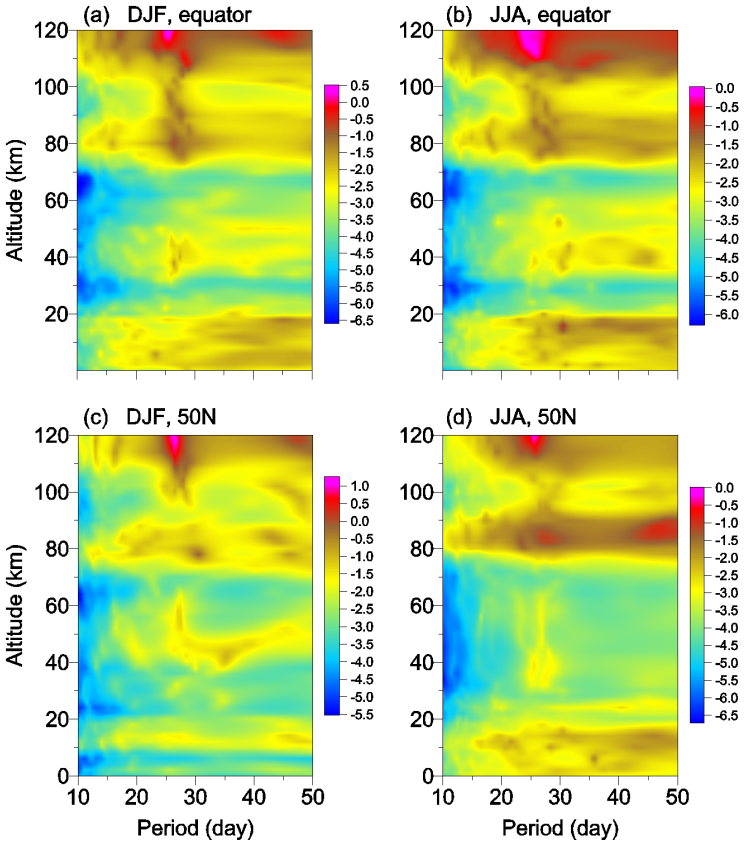

Fig. 5. Logarithm of the seasonal mean spectral density of the relative ozone content (ozone mixing ratios divided by its 5-year average values for the same altitude) as a function of altitude for **(a)** December–February at the equator, **(b)** June–August at the equator, **(c)** December–February at 50° N, and **(d)** June–August at 50° N. Units of spectral density: day.

ACPD
8, 1113–1158, 2008

EGU

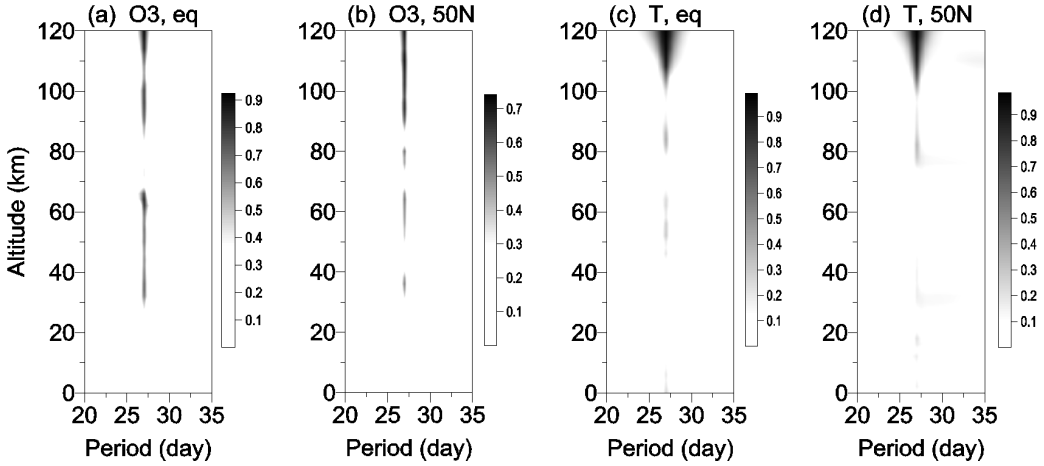

Fig. 6. Altitude distributions of the squared coherence spectra calculated between the 27-day forcing and **(a)** ozone at the equator, **(b)** ozone at 50° N, **(c)** temperature at the equator, and **(d)** temperature at 50° N, respectively.

ACPD
8, 1113–1158, 2008

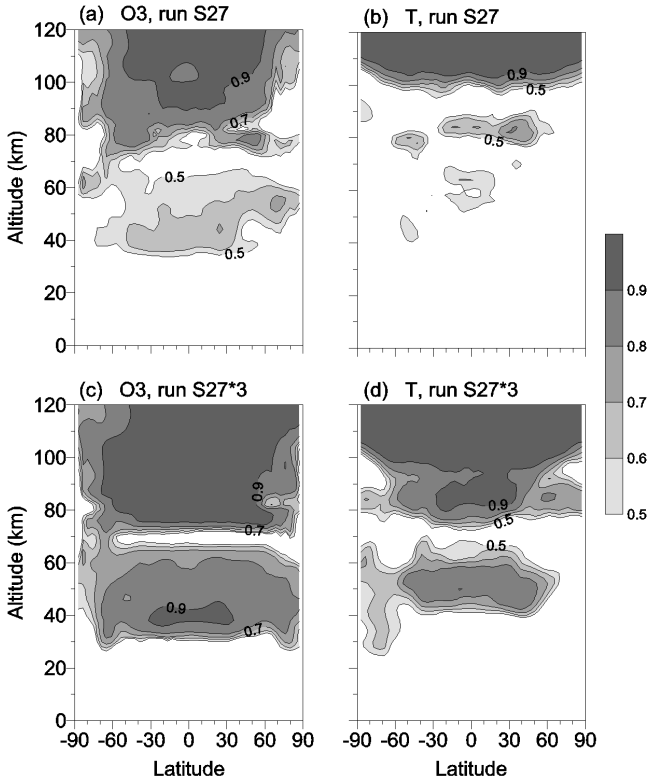

Fig. 7. (a, b) Altitude-latitude distributions of the squared coherence calculated between the standard 27-day forcing and (a) ozone, and (b) temperature, respectively. **(c, d)** As (a, b) but for the case of enhanced 27-day solar forcing.

ACPD
8, 1113–1158, 2008

EGU

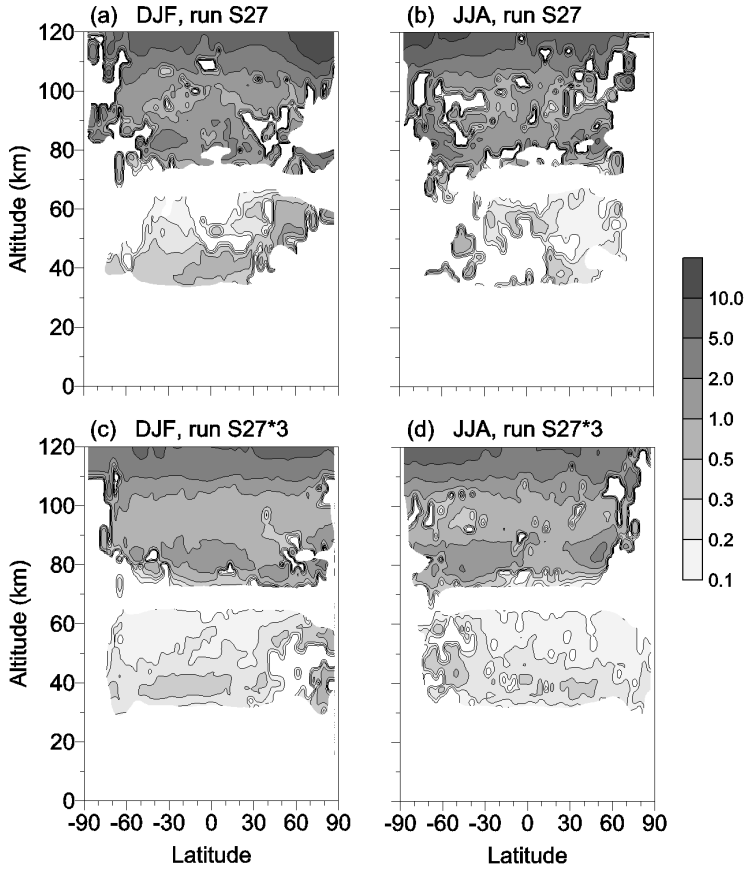

Fig. 8. (a–d) Altitude-latitude distributions of the ozone sensitivity to (a, b) standard and (c, d) enhanced 27 day solar forcing during (a, c) December–February and (b, d) June–August. Units: %/(%change of 205 nm irradiance).

ACPD
8, 1113–1158, 2008

EGU

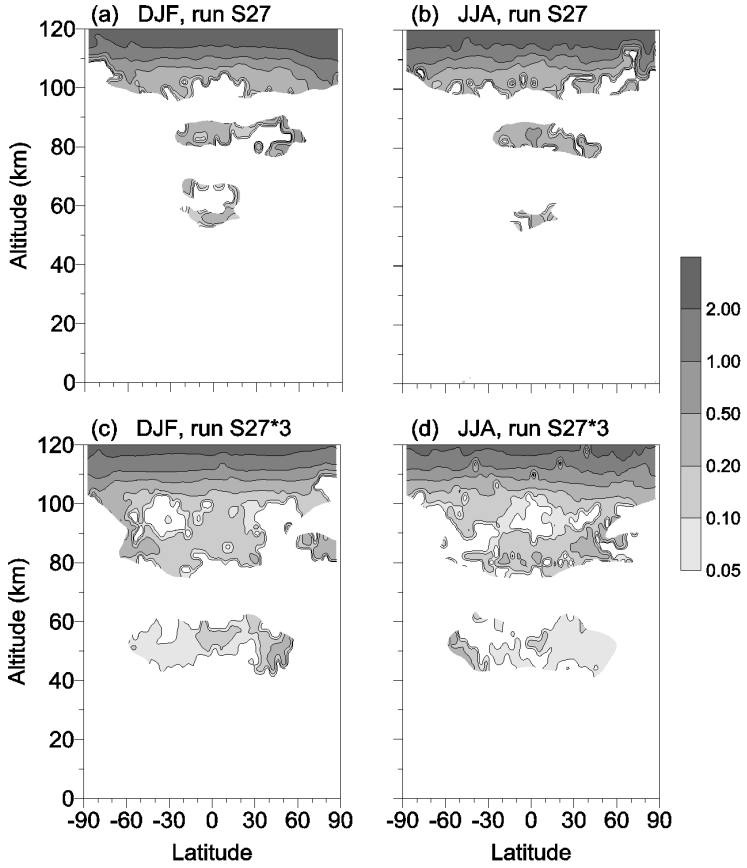

Fig. 9. As Fig. 8 but for the case of temperature. Units: K/(% change of 205 nm irradiance).

ACPD
8, 1113–1158, 2008

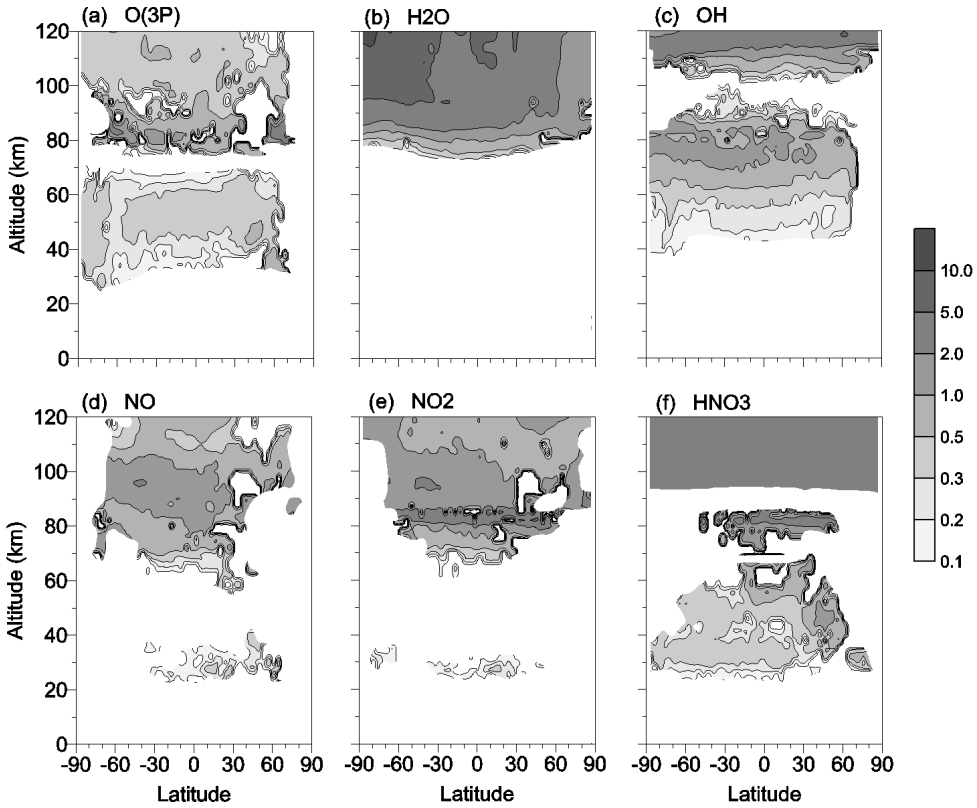

Fig. 10. Altitude-latitude distributions of the sensitivities of **(a)** $O(^3P)$, **(b)** water vapor, **(c)** OH, **(d)** NO, **(e)** NO_2, and **(f)** HNO_3 to enhanced 27 day solar forcing during December–February. Units: %/(%change of 205 nm irradiance).

ACPD
8, 1113–1158, 2008

EGU

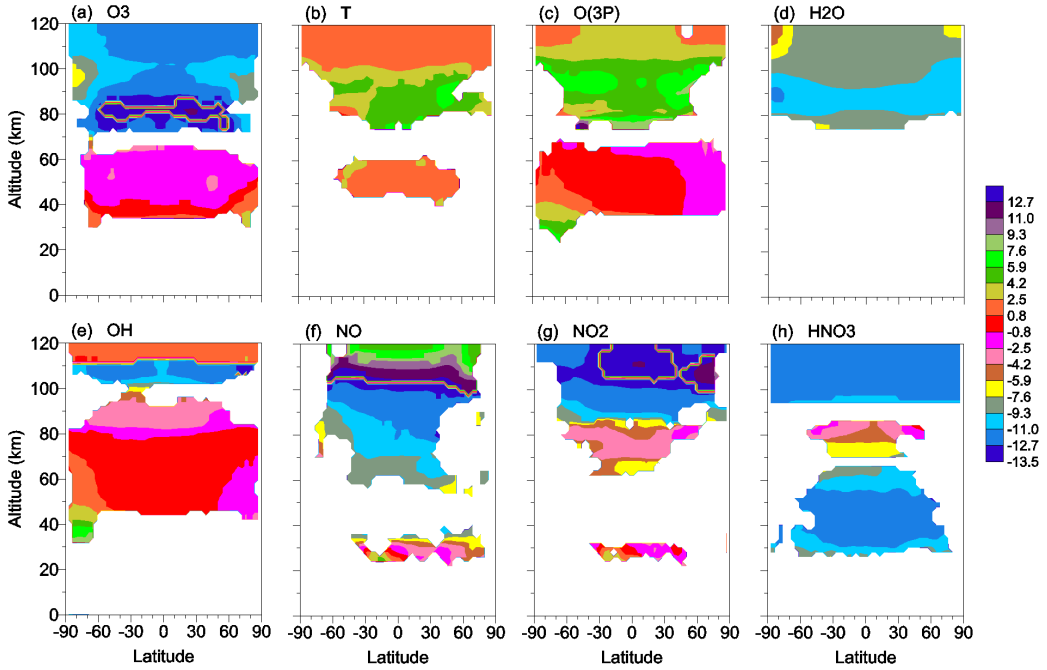

Fig. 11. Altitude-latitude distributions of the time lag of the **(a)** ozone, **(b)** temperature, **(c)** $O(^3P)$, **(d)** water vapor, **(e)** OH, **(f)** NO, **(g)** NO_2, and **(h)** HNO_3 responses to the 27-day solar forcing. Units: day.

ACPD
8, 1113–1158, 2008

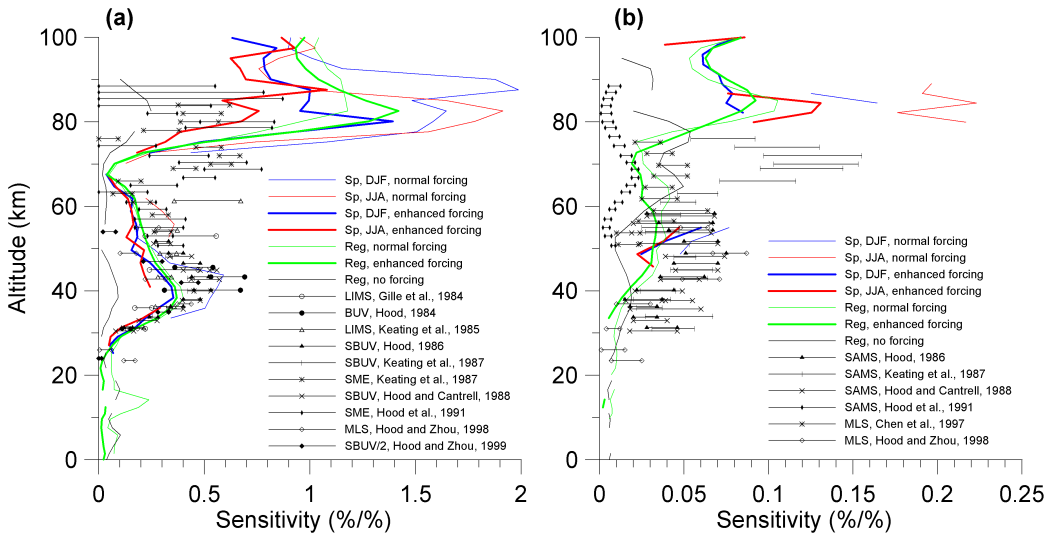

Fig. 12. Comparison of **(a)** ozone and **(b)** temperature sensitivities %/(% change of 205 nm irradiance) to 27-day solar forcing calculated by the model for 20° S–20° N latitude band (color and black curves) with observations in the tropical region (horizontal bars). Blue and red curves correspond to sensitivities derived by the spectral analyses for December–January and June–August, respectively, for the cases of standard (thin blue and red curves) and enhanced (thick blue and red curves) forcing. Green and black curves correspond to sensitivities derived by the linear regression analysis for the full year period for the cases of standard (thin green curve) and enhanced (thick green curve) forcing, and for the case without forcing (thin black curve). In the last case, the standard forcing amplitude was assumed to derive sensitivities. Shown are only values that are statistically significant at the 95% level. Horizontal error bars depict standard deviations. Note that the sensitivity unit for temperature differs from those used in Fig. 9.

ACPD
8, 1113–1158, 2008

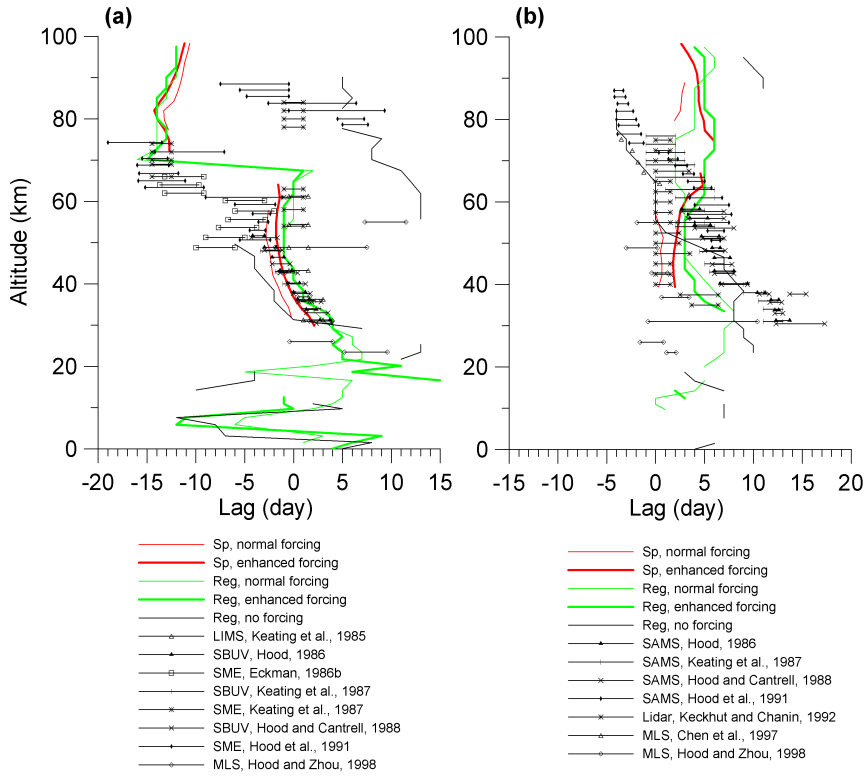

Fig. 13. Comparison of the time lags of the **(a)** ozone and **(b)** temperature responses calculated by the model for 20° S–20° N (color and black curves) with observations in the tropical region (horizontal bars). Red curves correspond to the lags derived by the cross-spectral analysis, green curves correspond to the lags derived by the linear correlation analysis for the cases of standard (thin red and green curves) and enhanced (thick red and green curves) forcing. Black curves correspond to the lags of the "response" obtained by the linear correlation method for the case without 27-day forcing.

ACPD
8, 1113–1158, 2008